batteries

MDPI

Article

Unravelling Lithium Interactions in Non-Flammable Gel Polymer Electrolytes: A Density Functional Theory and Molecular Dynamics Study

Nasser AL-Hamdani [1], Paula V. Saravia [2,3], Javier Luque Di Salvo [2,3], Sergio A. Paz [2,3] and Giorgio De Luca [1,*]

[1] Institute on Membrane Technology, ITM-CNR, Ponte P. Bucci, Cubo 17/c, 87036 Rende, Italy; n.alhamdani@itm.cnr.it
[2] Departamento de Química Teórica y Computacional, Facultad de Ciencias Químicas, Universidad Nacional de Córdoba, Córdoba X5000HUA, Argentina; pauvsaravia@unc.edu.ar (P.V.S.); javier.luquedisalvo@mi.unc.edu.ar (J.L.D.S.); apaz@unc.edu.ar (S.A.P.)
[3] Consejo Nacional de Investigaciones Científicas y Técnicas (CONICET), Instituto de Investigaciones en Fisicoquímica de Córdoba (INFIQC), Córdoba X5000HUA, Argentina
* Correspondence: g.deluca@itm.cnr.it

Abstract: Lithium metal batteries (LiMBs) have emerged as extremely viable options for next-generation energy storage owing to their elevated energy density and improved theoretical specific capacity relative to traditional lithium batteries. However, safety concerns, such as the flammability of organic liquid electrolytes, have limited their extensive application. In the present study, we utilize molecular dynamics and Density Functional Theory based simulations to investigate the Li interactions in gel polymer electrolytes (GPEs), composed of a 3D cross-linked polymer matrix combined with two different non-flammable electrolytes: 1 M lithium hexafluorophosphate ($LiPF_6$) in ethylene carbonate (EC)/dimethyl carbonate (DMC) and 1 M lithium bis(fluorosulfonyl)imide (LiFSI) in trimethyl phosphate (TMP) solvents. The findings derived from radial distribution functions, coordination numbers, and interaction energy calculations indicate that Li^+ exhibits an affinity with solvent molecules and counter-anions over the functional groups on the polymer matrix, highlighting the preeminent influence of electrolyte components in Li^+ solvation and transport. Furthermore, the second electrolyte demonstrated enhanced binding energies, implying greater ionic stability and conductivity relative to the first system. These findings offer insights into the Li^+ transport mechanism at the molecular scale in the GPE by suggesting that lithium-ion transport does not occur by hopping between polymer functional groups but by diffusion into the solvent/counter anion system. The information provided in the work allows for the improvement of the design of electrolytes in LiMBs to augment both safety and efficiency.

Keywords: lithium metal batteries; gel polymer electrolytes; Li^+ interactions; Li^+ solvation; molecular dynamics; density functional theory

Academic Editors: Pascal Venet, Zhi Wang, Tong Liu and Mingzhi Jiao

Received: 30 September 2024
Revised: 29 December 2024
Accepted: 9 January 2025
Published: 14 January 2025

Citation: AL-Hamdani, N.; Saravia, P.V.; Luque Di Salvo, J.; Paz, S.A.; De Luca, G. Unravelling Lithium Interactions in Non-Flammable Gel Polymer Electrolytes: A Density Functional Theory and Molecular Dynamics Study. *Batteries* **2025**, *11*, 27. https://doi.org/10.3390/batteries11010027

1. Introduction and Background

Lithium metal batteries are at the forefront of next-generation energy storage technologies, primarily due to their exceptional energy density and theoretical specific capacity, which significantly exceed those of conventional lithium-ion batteries with graphite anodes. Lithium metal has a theoretical specific capacity of 3860 mAh g^{-1}, compared to graphite's

capacity of 372 mAh g^{-1} [1,2]. This makes LiMBs a viable option for high-energy applications such as electric vehicles and large-scale energy storage systems [3,4]. In addition, the lightweight and high electrochemical potential of lithium metal makes it even more appealing for improving the overall energy efficiency of batteries [5].

However, the implementation of LiMBs in real-world scenarios is hindered by significant safety issues. One of the main concerns is the use of flammable organic liquid electrolytes, which carry a substantial risk of flammability, especially when exposed to high temperatures or in case of an internal short circuit [6,7]. Furthermore, the formation of lithium dendrites during the process of repetitive charging and discharging can result in short internal circuits and ultimately cause the battery to fail catastrophically [3–6]. These dendritic structures not only compromise safety but also reduce the lifespan and efficiency of the batteries, presenting a major obstacle to the widespread adoption of LiMBs technology [8,9].

To mitigate these issues, recent advancements have focused on the development of gel polymer electrolytes (GPE), which integrate the advantages of both liquid and solid-state electrolytes. A key innovation in this domain is the use of dendrimers—highly branched, tree-like polymers with well-defined structures. These polymers offer precise control over the electrolyte architecture, enhancing both mechanical stability and ionic conductivity [10,11]. Their non-stackable nature prevents undesirable phase separation and ensures uniform ion distribution, addressing critical challenges such as dendrite formation and electrolyte instability [12–14]. Moreover, dendrimers can be functionalized with various groups to further enhance the performance and safety of GPEs [14–16].

In this framework, the work, recently published by Hu et al. [15], is particularly interesting. In their work, a multifunctional, all-in-one gel polymer electrolyte membrane with a 3D cross-linking network was synthesized with the aim of creating polymer electrolyte membranes with 3D cross-linking networks that improve both performance and safety. The proposed GPE integrates -CN and -$PO(OC_2H_5)_2$ functional groups into a single polymer matrix, formed by acrylonitrile (AN) and diethyl vinyl-phosphonate (DEVP) monomers, cross-linked by poly(ethylene glycol) diacrylate (PEGDA). This integration aims to produce a synergistic effect that enhances ionic conductivity, mechanical stability, and flame resistance. As highlighted by Hu et al. [15], the -CN groups enable the formation of stable Li3N-rich solid electrolyte interphase (SEI), which inhibited the proliferation of lithium dendrites, and high-quality cathode electrolyte interphase (CEI) layers that stabilize the $LiFePO_4$ cathode. Moreover, the addition of -$PO(OC_2H_5)_2$ functional groups improved the flame resistance of the electrolyte, thereby decreasing the likelihood of combustion by capturing reactive radicals. Hence, the combined effect of these functional groups in a 3D cross-linking polymer network showed significant enhancements in both electrochemical performance and safety, showing the need to design at the molecular level more sophisticated, dependable, and safe LiMBs. This GPE is innovative because it combines synergistic advantages not commonly observed in other comparable systems used in Li metal batteries. Therefore, this cross-linked GPE deserves notable attention. To date, no theoretical studies have explored the impact of the various components of this GPE. This underscores the significance of our work, as it provides critical insights that can be used to optimize this novel system.

Despite significant advancements in the development of gel polymer electrolytes, there is still a lack of comprehensive understanding of the molecular-level behavior of the lithium ions in these systems. The transport of Li^+ is affected by various crucial parameters, including the coordination between lithium cations and functional groups present in the polymer matrix, as well as the structural arrangement of the GPE [3–10]. Previous theoretical studies, such as those by Wróbel et al. [17], have investigated the solvation

dynamics of lithium ions in various solvents, emphasizing the role of solvent interactions in facilitating Li^+ transport. Similarly, Tasaki [18] explored the decomposition mechanisms and interactions of lithium ions in electrolytic environments through DFT calculations and molecular dynamics simulations, highlighting the significance of these interactions on overall battery performance. Additionally, research by Haskins et al. [19] has provided insights into the electronic structure and transport properties of lithium-doped ionic liquids, further informing the understanding of ion mobility in polymer systems. Nevertheless, the specific molecular interactions and pathways that control ion mobility in GPE are not well comprehended, which makes it difficult to optimize these membranes to meet the demanding performance and safety criteria for future LiMBs [4–18].

This study aims to address the knowledge gap by examining the interactions between Li^+ and the components of the novel 3D cross-linked polymer electrolyte (3D-ADCL-PE) proposed by Hu et al. To achieve this goal, two distinct solvent systems are analyzed: (E_1) 1 M Lithium hexafluorophosphate ($LiPF_6$) in ethylene carbonate (EC)/dimethyl carbonate (DMC) solvent, originally used to test the 3D-ADCL-PE polymer [15], and (E_2) 1 M Lithium bis(fluorosulfonyl)imide (LiFSI) in trimethyl phosphate (TMP) solvent, which is known for its potential in developing high-safety rechargeable Li batteries, including both LiBs and LiMBs [20,21]. These electrolytes were chosen to evaluate the influence of different ionic environments on Li^+ coordination with solvent molecules and counter-anions within the GPE.

Advanced Molecular Dynamics (MD) and Density Functional Theory (DFT) simulations are carried out to assess the Li^+ interactions and how the components affect Li^+ transport [17–23]. MD simulations capture the motions of ions and polymer chains throughout time. From MD trajectories, we can extract frames of structures (snapshots) for further accurate quantum mechanical calculation of the interactions experimented by Li^+, guaranteeing precise outcomes in the subsequent stage of the investigation [17–19]. Building on these MD simulations, DFT calculations provide energies associated with interactions between Li^+ and GPE components. The Li^+ interactions linked to their distribution in the non-stackable gel polymer electrolytes were studied to understand how these molecular interactions govern key electrolyte properties, including conductivity and stability. The combined MD and DFT simulations provide a complete approach to understanding at the molecular scale the GPE behavior. While MD sets up accurate structures as a function of time, DFT delves into quantum aspects, revealing key insights correlated to ion transport in the GPE. This study is useful to receive a more profound comprehension of the transport mechanisms at the molecular level to achieve further optimization of these systems. This research intends to support the design of new materials with optimized functional groups and the development of sustainable and eco-friendly battery technologies by reducing the need for extensive experimental testing [14–19].

2. Computational Approach

2.1. Preparation of GPE Systems

The gel polymer electrolyte proposed by Hu et al. [15] was used as a reference. The polymer model was composed of 820 acrylonitrile (AN) and 270 diethyl vinyl-phosphonate (DEVP) monomers, in addition to 5 poly(ethylene glycol) diacrylate (PEGDA) units used as cross-linkers, shown in Figure 1. The polymer was generated from its monomers and cross-linkers using the HTPolyNet Python package [24–27]. From monomer structures and topologies describing the chemistry of any linking reactions, HTPolyNet builds the appropriate parameter set and initiates a capture-radius-based bond-formation step with relaxation, performing short MD simulations in Gromacs [27] with simultaneous updating of bonding topology.

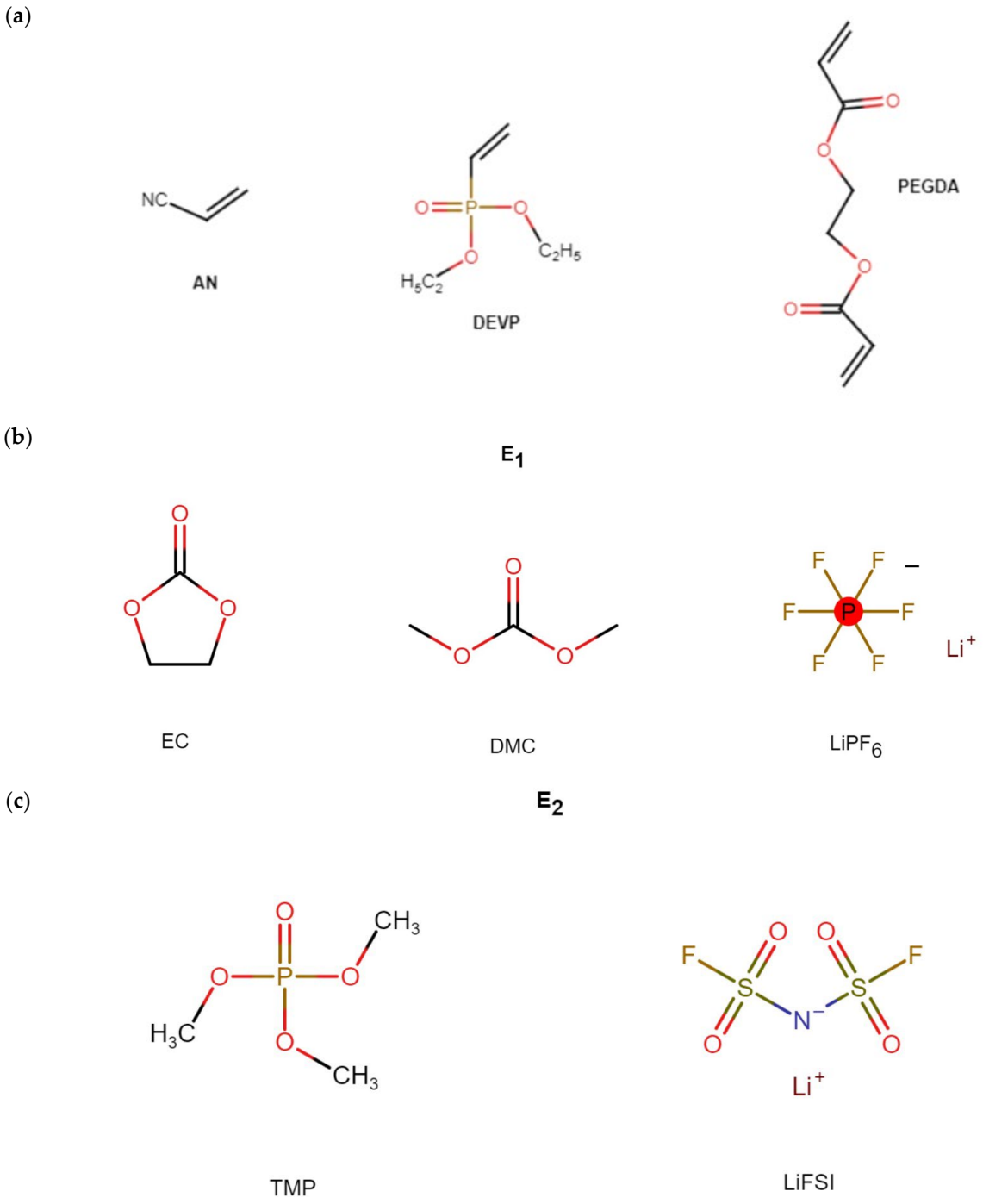

Figure 1. (**a**) Monomer structures of the 3D-ADCL-PE; (**b**,**c**) structures of the solvents and salts used as electrolytes: E_1 and E_2, respectively.

The obtained cross-linked matrix was a dense system of 3D cross-linked polymers with a final density of 1.11 g/cm^3 without electrolytes. Moreover, in order to improve the polymer model, it was subjected to NPT for 10 ns at very low pressure (0.01 bar) to lower the density of the dried polymer and then facilitate the random insertion of electrolytes. Finally, the 3D cross-linked polymer and tested electrolytes were equilibrated for at least 200 ns NPT at 1 bar. The equilibrated GPE box has a 5.92 nm length in each simulation box axis. Full details on the molecular dynamics simulations adopted for the 3D cross-linking step and the liquid electrolyte insertion are given in the Supplementary Materials.

Two different electrolytes, whose structures are shown in Figure 1b,c, were studied in order to assess the effect of solvents and salts. The final systems, E_1 and E_2, consisted

of 3D-ADCL-PE, 266 DMC molecules, 340 EC molecules, 90 Li^+ and 90 PF_6^- (E_1) along the polymer matrix, and 427 TMP, 50 FSI, and 50 Li^+ ions (E_2). The number of solvent molecules and salt ions for E_1 corresponds to 1M $LiPF_6$ in DMC:EC 1:1 v/v mixture as adopted in the experimental reference to prepare the GPE [15]. Likewise, the number of solvent molecules and ions for E_2 corresponds to electrolyte solution 1M LiFSI in TMP. Based on the reported electrolyte uptake by the polymer of 298.7 wt.% with a porosity of 65.8%, a polymer/electrolyte weight ratio corresponding to 80 wt.% was adopted in order to take into account without overestimation only the swelled polymer region and exclude the liquid entrapped within the larger pores; in doing this, we assume a homogenous distribution of liquid electrolyte within/near the polymer chains and in the pores.

In order to obtain representative atomic clusters for the subsequent DFT calculations, radial distribution functions (RDF) and the corresponding cumulative coordination numbers (CN) were evaluated by averaging the trajectories over the last 100 ns. Then, the first peak of each RDF was used as a reference for the most probable Li-X distance, with X = N (-CN), O (DEVP), and P (DEVP), referring to atoms of the polymer monomers, respectively, and X = O (DMC), O (EC), F (PF_6^-), and O (TMP), O (FSI), N (FSI), and F (FSI), referring to E_1 and E_2 O, P, and F atoms of the two analyzed electrolyte compositions, respectively. The all-atom General Amber Force Field (GAFF) parameters [28], which have been used in the literature to model similar gel polymer electrolytes [29], were used to model the cross-linked polymer, solvent molecules, as well as the anions and Li^+. This force field was chosen due to its generality in describing interactions between a broad variety of components that make the GPE of our study: polymers with different functional groups, solvent molecules, and ions. This allows us to effectively model the specific system under study considering the two electrolytes chosen in this work, and at the same time, it opens the room for easy transferability to other similar systems.

Radial distribution functions are defined as the probability density of finding a B atom at a distance r from a reference A atom, normalized by the local density of B atoms in the system,

$$g_{AB}(r) = \frac{1}{\langle \rho_B \rangle_{local}} \frac{1}{N_A} \sum_{i \in A}^{N_A} \sum_{i \in B}^{N_B} \frac{\delta(r_{ij} - r)}{4\pi r^2} \quad (1)$$

where $g_{AB}(r)$ is the RDF, $\langle \rho_B \rangle_{local}$ is the average local number density of B atoms, N_A and N_B are the number of atoms of type A and B, respectively, and $\delta(r_{ij} - r)$ is the Dirac delta function, ensuring contributions only when the distance $r_{ij} = r$.

The cumulative coordination number is obtained by integrating the RDF over the range from 0 to a specific distance D,

$$CN\ (D) = 4\pi \langle \rho_B \rangle_{local} \int_0^D r^2 g_{AB}(r) dr \quad (2)$$

While the RDF provides the local probability distribution of an atom type, the CN offers a cumulative measure, giving complementary insights into the solvation structure.

It is important to note that the smoothness of the RDF curves in this study arises naturally from averaging over the 100 ns trajectory data. While RDFs are theoretically defined using a Dirac delta function to count pairwise distances exactly at r, practical implementations group distances into small bins through histogram binning [30].

When the RDF is calculated for a single snapshot, the limited number of atom pairs contributing to each bin results in noisy fluctuations. However, by averaging over the entire trajectory, the bins are populated with contributions from numerous pairs across time, leading to smoother curves. This standard approach provides reliable statistics and accurately represents the system's equilibrium behavior.

Finally, it is important to emphasize that the deep analysis of the averaged RDFs is important to understand what the chemical environment around the target Li ion in this GPE is, hence, to decide which atomic clusters should be considered in the quantum calculation of the interaction energy.

2.2. Interaction Energy Calculation

The clusters for quantum calculations were extracted based on RDF analysis. As will be demonstrated in Section 3, RDFs revealed that cations predominantly interact with solvent molecules and counter-anions, rather than the polymer matrix. Thus, the clusters were constructed following these observations, ensuring a focus on the solvent and counter-anion interactions surrounding Li^+.

Overall, four clusters were extracted. Clusters C-E_1 and C-E_2 consisted of different Li cations surrounded by cross-linked polymer chains and solvent molecules without PF_6^- or FSI^- counter-anions. Instead, $C_{PF6}{}^-$-E_1 and $C_{FSI}{}^-$-E_2 included lithium ions, polymer chains, and counter-anions. The average total number of atoms included in each cluster is 310. The preparation of the clusters was carried out by identifying Li^+ ions that adhered to the observed RDF behavior, i.e., Li^+ that consistently resided near solvent molecules and counter-ions. It is important to emphasize that the RDF analysis showed the absence of close interactions between Li^+ and the polymer matrix's functional groups (N from AN, O, or P from DEVP), as Li^+ ions were constantly found in proximity to solvent or counter-anion molecules, which act as a shield between Li^+ and polymer chains. Finally, in order to capture the surrounding atomic environment, all atoms within a radius of 1 nm from a target Li^+ were included in the clusters. Remember that the dimension of the complete equilibrated GPE box is 5.92 nm.

After the clusters were extracted, quantum calculations were performed using Density Functional Theory (DFT) with the Northwest Computational Chemistry Package (NWChem 6.6) [31]. Calculations were carried out for both closed-shell and open-shell configurations, with a multiplicity of 2 for open-shell structures. The B3LYP exchange-correlation functional [32] was employed with Grimme's D4 dispersion correction. The self-consistent field (SCF) energy convergence criterion was set to 5×10^{-6} a.u., with a root mean square (RMS) electron density convergence of 1×10^{-5} a.u.

Different basis sets were used for the atoms in each cluster to balance computational efficiency and accuracy. Specifically, a split-valence double ζ basis set with polarization functions (6–31G*) was applied to lithium and atoms directly interacting with Li^+ using the cut-off distance for defining interactions equal to 0.3 nm [33]. While the remaining atoms in the clusters were treated with a standard split-valence double-ζ basis set (4–31G) to optimize computational performance.

Lithium-ion interaction energies were calculated according to the following equation:

$$\Delta E_{int} = Ener_1 - Ener_2 - E_{Li^+}, \quad (3)$$

where $Ener_1$ is the energy of the atomic cluster containing the target Li^+, $Ener_2$ is the energy of the cluster without these cations, while E_{Li^+} is the energy of the target Li^+ alone, placed in the position found in the cluster. It is worth noting that in the considered clusters, more Li ions were found, which determine the total charge of the cluster; however, ΔE_{int} was calculated for the central Li^+ indicated as the target. Furthermore, to enhance the accuracy of the computed energies referred to the interaction between the Li^+ and their surrounding environment, basis set superposition error [34] (BSSE) adjustments were applied utilizing the counterpoise approach. BSSE is important as it facilitates a more precise assessment of the interaction energy by removing irrelevant contributions from basis set deviations [35]. An overview of the simulation protocol of the GPE can be seen in Scheme 1 below.

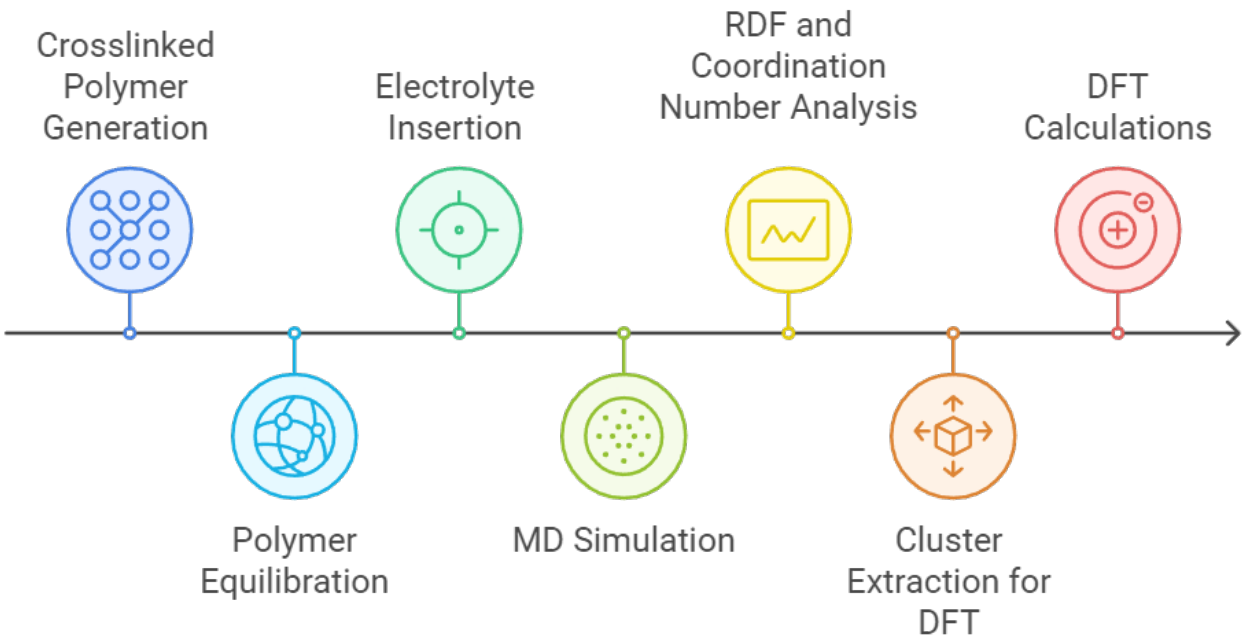

Scheme 1. A diagram illustrating the process flow and stages involved in the simulation.

3. Results and Discussion

3.1. Li^+ Surrounding Environment Through RDF and CN Analyses

This study aimed to investigate the structures and interactions preferred by Li ions in the novel 3D cross-linked polymer electrolyte. MD simulations were first performed to elucidate the Li^+ coordination environments by analyzing the RDFs and CNs obtained from the equilibrated GPE models, shown in Figure 2. The obtained density of the modeled GPEs is 1225 and 1220 kg/m^3 for E_1 and E_2 systems, respectively.

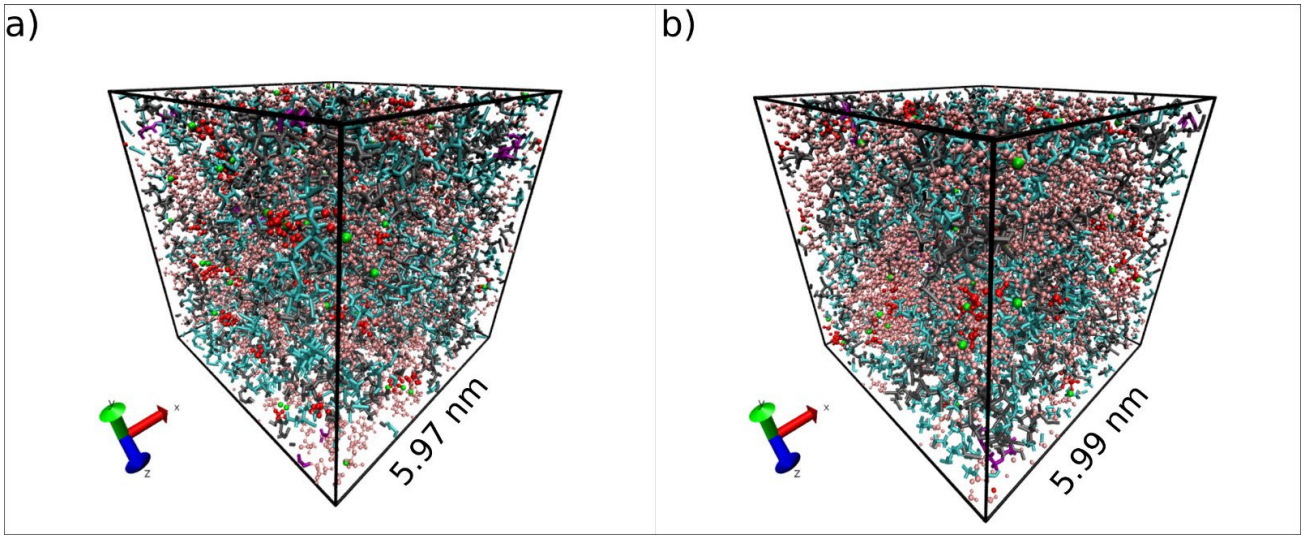

Figure 2. MD equilibrated GPE: (**a**) 3D cross-linked polymer plus 1 M Li PF_6 in EC/DMC; (**b**) 3D cross-linked polymer and 1 M LiFSI in TMP. Boxes are cubic and have the same dimensions in all xyz coordinates.

Figure 3 presents the RDFs for the E_1 system. Figure 3a displays the radial distribution functions for the distances between Li^+ and the key atoms in the electrolyte, while Figure 3b focuses on the RDFs for the polymer matrix. As can be seen in these figures, no peaks were observed below 0.5 nm for the distances between Li^+ ions and N, O, or P atoms of the

polymer functional groups. Instead, peaks below this threshold exclusively correspond to interactions between Li^+ and PF_6^-, EC, or DMC. In particular, the RDFs in 3a show strong, well-defined peaks at 0.2 nm associated with the most probable distance between Li^+ and oxygen atoms of the solvent molecules, as well as fluorine atoms from PF_6^-. These results highlight that Li^+ forms stable solvation shells primarily with these mobile components of the GPE. Figure 3b also shows that the RDFs for distances between Li^+ and functional group atoms of the polymer matrix remain zero up to 0.5 nm, only increasing slightly beyond this distance. This is further supported by the broader and less defined curves, indicative of weaker interactions. This means that, during the last 100 ns of the MD simulation, the Li^+ ions are more likely interacting with solvent molecules or PF_6^- than with the functional groups of the 3D cross-linked polymer matrix. This behavior can be attributed to the lower mobility of the 3D cross-linked polymer compared to the solvent molecules, which can dynamically arrange around the Li^+ ions in greater numbers, forming stable solvation shells.

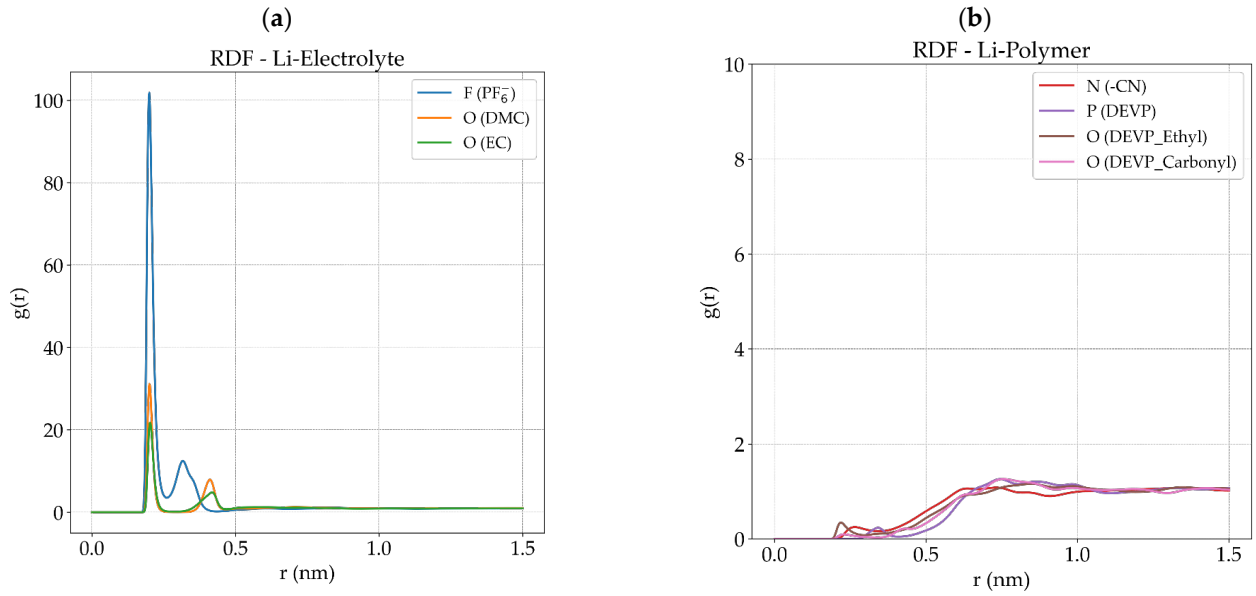

Figure 3. (**a**) Li-X RDFs associated with all interatomic distances among Li ions and atoms of the GPE-E_1 electrolyte components; (**b**) RDF associated with the atoms of the functional groups of the cross-linked polymer.

The CN as a function of the Li-X distance confirms this conclusion. The CN plots allow the direct comparison of how many atoms, on average, are at a certain distance from Li^+ thus giving an idea of its coordination shell. Figure 4a shows that the coordination numbers for the electrolyte components (Li^+-PF_6^-, -EC, and -DMC) remain zero up to 0.2 nm, after which the CN curves increase rapidly. While the CN profiles, related to the atoms of polymer functional groups (Figure 4b), remain at zero up to 0.5 nm and increase afterwards. It should be stressed that g(r) is normalized by the number of atoms and not the number of molecules/ions; thus, at r = 0.5 nm, the CN for Li-F(PF6), Li-O(DMC), and Li-O(EC) are 7.1, 4.7, and 5.1, respectively, indicating the presence of roughly 1 PF6 anion and 3 solvent molecules (the Li-O RDF curves capture the three oxygen atoms per solvent molecule) around Li^+ within 0.5 nm. These trends confirm that DMC, EC, and PF_6^- are the primary contributors to the Li^+ solvation structure. The CN plots make this result apparent, i.e., lower coordination numbers for -CN and -$PO(OC_2H_5)_2$ for short-range distance (at bond length) from Li^+, suggesting that the polymer matrix contributes minimally to Li^+ solvation in this GPE.

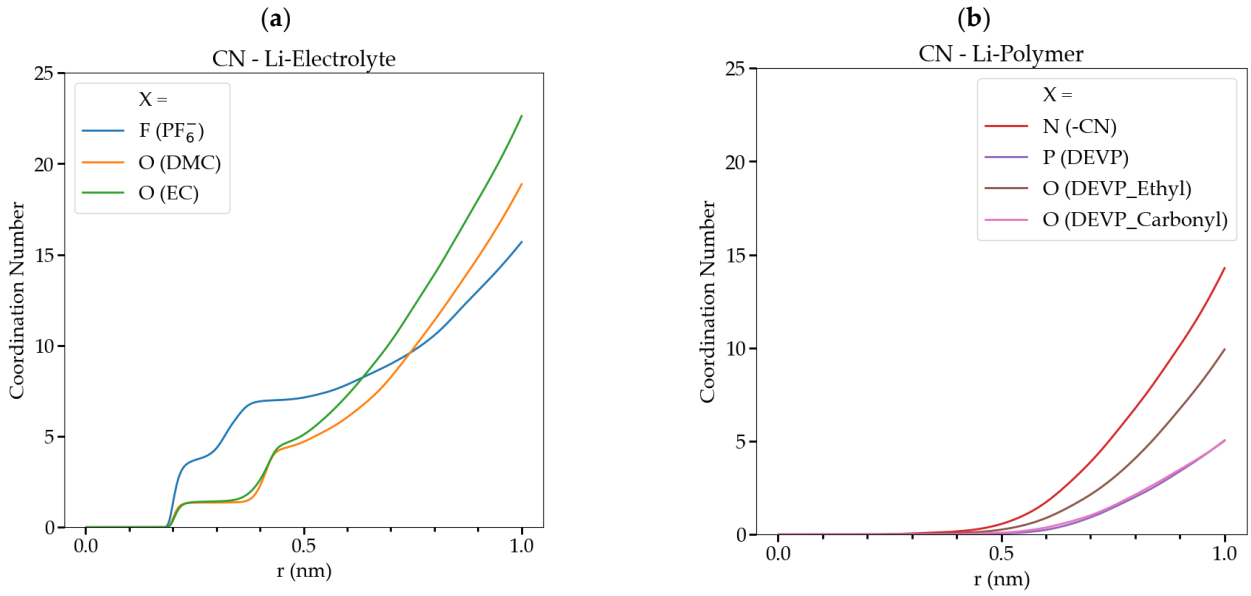

Figure 4. (**a**) CN associated with all atoms interacting with Li^+ in GPE E_1 for the electrolyte atoms; (**b**) CN of the atoms of the functional groups of the cross-linked polymer.

The RDF profiles for the E_2 systems, shown in Figure 5, demonstrate trends that are similar to those found for the E_1 polymer electrolyte in Figure 4. In detail, in Figure 5a (RDF for Li-Electrolyte), sharp peaks in yellow and blue colors at 0.19 nm and 0.21 nm can be noticed, respectively, which reveal strong interactions between Li ions and the oxygen atoms of the FSI counter-anion and solvent molecules. Furthermore, at 0.23 nm and 0.40 nm, two more marked peaks in red and green are observed, which indicates that the other probable atoms closer to the Li cations are N and F of the FSI. As for the previous E_1, no peak corresponding to interatomic distances between Li^+ and functional group atoms of the polymer was found below 0.5 nm (Figure 5b); only a broader line appears above this threshold. The RDFs plots reveal that Li^+ preferentially interacts with electrolyte components, specifically the oxygen atoms of FSI and TMP as well as the fluorine and nitrogen atoms of the counter-anion. Again, the CN profiles reported in Figure 6 confirm this finding. The oxygen TMP-related coordination number increases significantly after 0.2 nm, hence the oxygen-associated coordination number of FSI, underscoring their importance in the formation of the solvation shell around Li^+. In particular, the CN plots indicate that within 0.5 nm, Li^+ is coordinated by roughly 1 anion and 3 solvent molecules. Meanwhile, the CN trends for the functional group atoms exhibit weaker and more diffuse interactions, similar to the E_1 system, further highlighting the minimal role of the polymer in Li^+ solvation. Detailed RDF and CN profiles for each target atom can be found in the Supplementary Materials.

Overall, a coherent picture emerges in which both GPE and Li^+ strongly favor interactions with the electrolyte components—the solvent molecules (DMC, EC, and TMP) and counter-anions (PF_6^- and FSI^-)—over the polymer matrix. The solvation shells formed by these components are critical for efficient Li^+ transport. It should be noted that the RDF and CN analyses do not provide the extent of the interactions between cation and electrolyte components, but they do provide a picture of the environment surrounding the ions in the GPEs. To obtain the strength of the Li^+ interactions, DFT calculations were carried out in the next section using snapshots obtained from the MD simulations based on the results coming from the RDF and CN analysis.

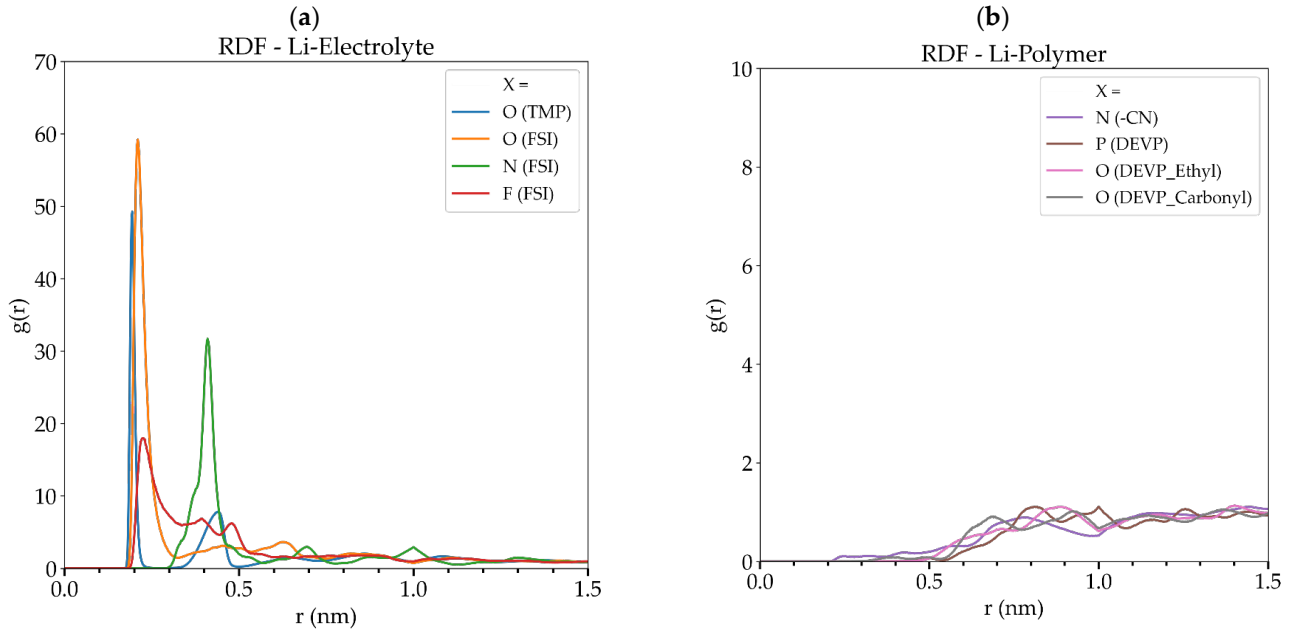

Figure 5. (**a**) Li-X RDFs associated with all inter-atomic distances among Li ions and atoms of the GPE E_2 for electrolyte components; (**b**) RDF associated with the atoms of the functional groups of the cross-linked polymer.

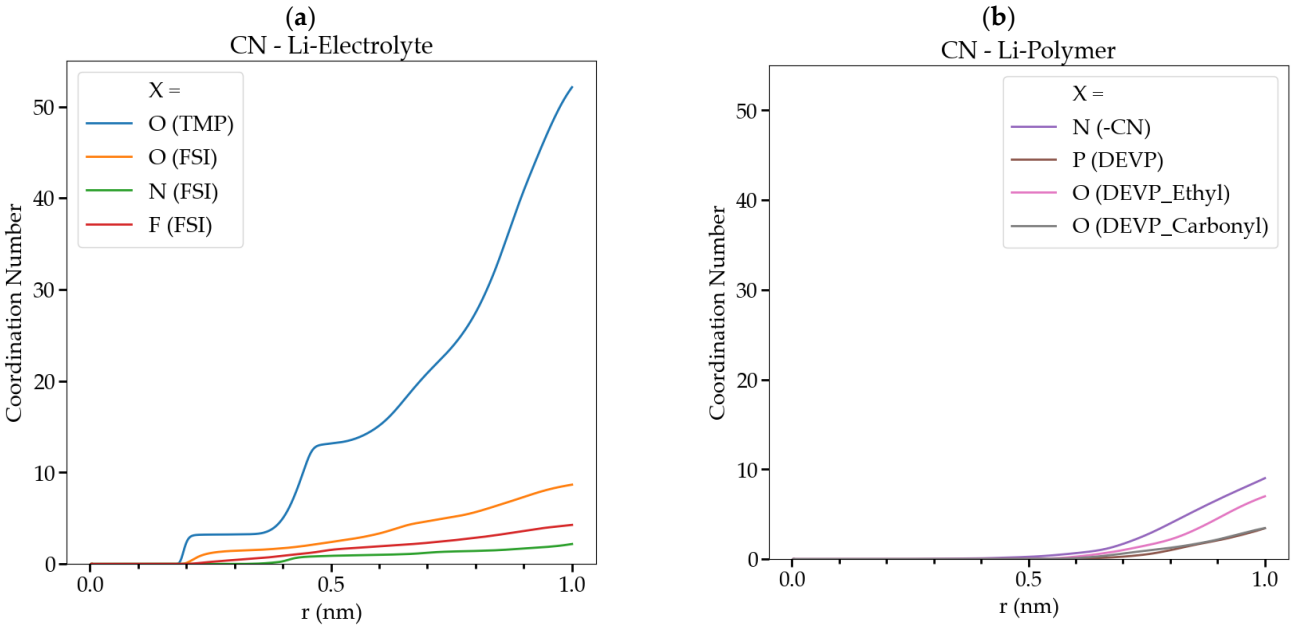

Figure 6. (**a**) CN associated with all the atoms interacting with Li^+ in GPE E_2. for the electrolyte atoms and (**b**) CN of the atoms of the functional groups of the cross-linked polymer.

3.2. Interaction Energies of Li Ions in GPE

MD simulations provided information on the most likely chemical environment experienced by Li ions in the cross-linked GPE. From these simulations, we extracted four representative atomic clusters shown in Figure 7, each depicting distinct solvation environments surrounding the Li^+ and used them to evaluate the interaction energies ΔE_{int}. The first cluster (C-E_1, Figure 7a) comprises Li^+ primarily interacting with adjacent solvent molecules, while in the second one ($C_{PF6}{}^-$-E_1, Figure 7b), the short-range interactions with both solvent and counter-anion species were considered. Furthermore, similar clusters

associated with the E_2 composition were extracted from the MD trajectories (C-E_2, $C_{FSI}{}^{-}$-E_2, Figure 7c,d).

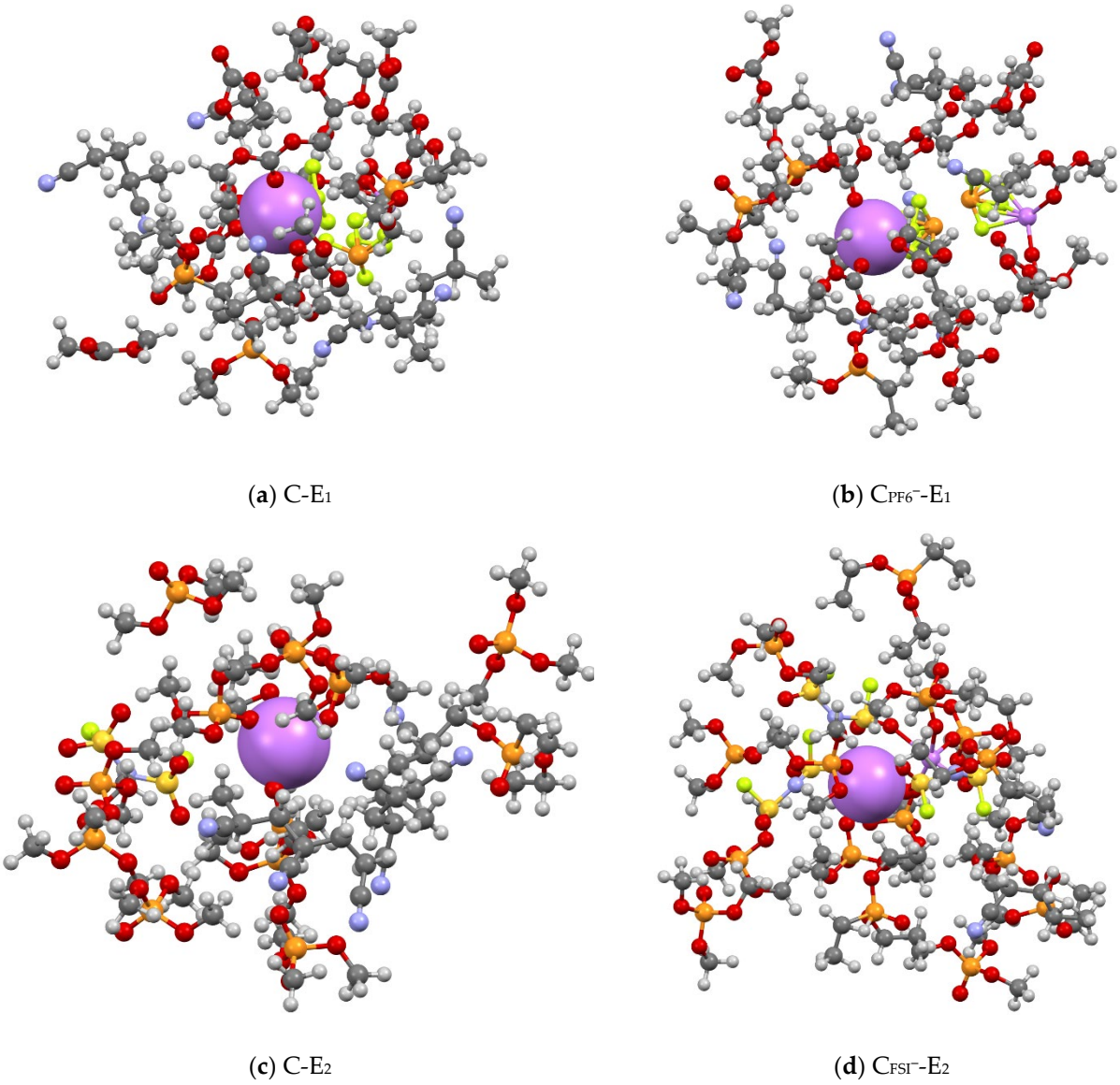

(**a**) C-E_1 (**b**) $C_{PF6}{}^{-}$-E_1

(**c**) C-E_2 (**d**) $C_{FSI}{}^{-}$-E_2

Figure 7. Cluster structures extracted from MD equilibrated systems: (**a**) central Li^+ interacting at short distance with (EC:DMC) solvent, (**b**) central Li^+ interacting at short distance with (DMC:EC) solvent and $PF_6{}^-$ counter-anions, (**c**) Li^+ interacting with TMP solvent, and (**d**) interacting with TMP solvent and FSI^- counter-anions. All 4 clusters had parts of the polymer equilibrated box as well. Colors: Li^+ (violet), C (gray), H (white), O (red), F (yellow), and P (orange). Target Li ion is represented with its van der Waals radii while the rest are visualized by the ball-and-stick representation.

Efforts to identify clusters with locations near the functional group of the polymer matrix (-CN or DEVP) were ineffective, since, as demonstrated from RDFs and CN analysis, Li^+ continually remained near solvent molecules and counter-anions. As previously discussed, Li ions primarily engage with the electrolyte molecules instead of the polymer matrix, highlighting the preeminent influence of solvents and salts in solvation. Thus, these clusters offer insights into the binding characteristics of Li ions in the two electrolyte systems.

Although we were unable to find clusters in which Li^+ interacts at short distances (bond length) with polymer functional groups in agreement with RDFs analysis, the interaction energies evaluated according to Equation (3), and reported in Figure 8, take into consideration not only the molecules nearby to Li^+ but also the overall chemical environment, i.e., polymer fragments with the functional groups. Thus, the indirect effect of the polymer is taken into account in the ΔE_{int} values.

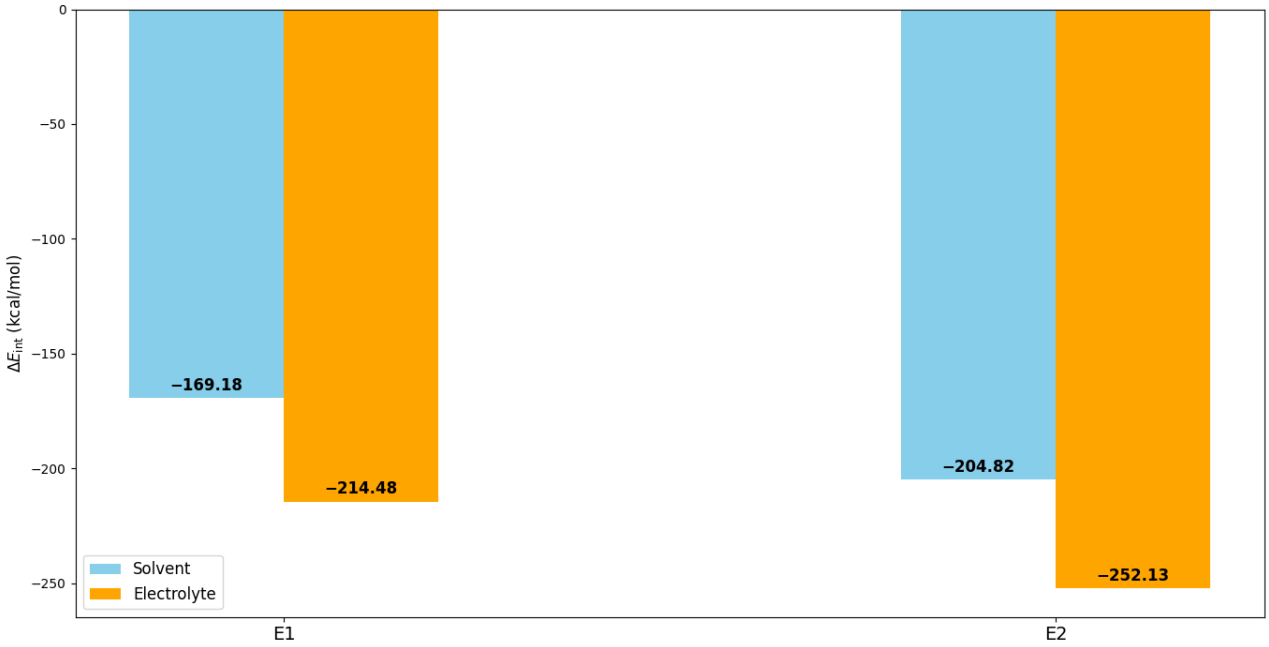

Figure 8. Li^+ interaction energies for E_1 and E_2 electrolyte compositions. The light blue column refers to the C-E_1 and C-E_2 clusters, while the orange column refers to the $C_{PF6}{}^-$-E_1 and $C_{FSI}{}^-$-E_2 ones.

As shown in Figure 8, the interaction energies referring to the two electrolyte systems show significant differences. In the E_1 system, the ΔE_{int} of Li^+ with the solvent (DMC/EC) was −169.18 kcal/mol, but the interaction with the whole electrolyte, i.e., incorporating the $PF_6{}^-$ counter anions, yielded a more substantial ΔE_{int} of −214.48 kcal/mol. This demonstrates that $PF_6{}^-$ plays a crucial role in the solvation shell surrounding Li^+. E_2 exhibited stronger interactions overall compared to E_1. The interaction energy between target Li^+ and solvent molecules (TMP) was −204.82 kcal/mol, but incorporating the effect of FSI^- counter anions further increased, in absolute value, the ΔE_{int} to −252.13 kcal/mol. The increased interaction energies in this system underscore the stabilizing influence of FSI^-, which surpasses that of $PF_6{}^-$ in the EC/DMC system.

The DFT results clearly show that the LiFSI/TMP system provides a more stable solvation environment than the $LiPF_6$/EC-DMC electrolyte. The stronger Li interaction energies in the FSI^-/TMP system suggest that Li ions form a more stable solvation shell, which could enhance the ion solvation from the SEI or CEI and then ionic conductivity. On the other hand, the weaker interactions in the $PF_6{}^-$/EC-DMC system suggest a more dynamic solvation shell, which might support faster ion mobility.

Insights from the RDF and CN analyses, as well as the ΔE_{int} values, offer a deeper understanding of Li^+ transport mechanisms at the molecular level. The absence of RDF peaks for Li-NC and Li-DEVP bond distances below 5 Å indicates that interactions between Li^+ and the functional groups of the cross-linked polymer do not hinder Li transport. Instead, the electrolytes directly interact with Li^+ ions, supporting a solution-diffusion mechanism for transport.

Based on the above consideration, a macroscopic solubility-diffusion mechanism is plausible; thus, Li^+ ion flux is governed by two primary factors: solvation and mobility. Solvation (S) is influenced by the interaction energies between ions and solvents/salts, while the mobility is correlated with the ion diffusion coefficient (D) depending on the activation energy for diffusion, which in turn depends on the overall interactions between the ion and its environment. Stronger solvent-Li interactions are not always advantageous. Depending on the strength of interactions among the solvent, counter ions, and polymer network, a more dynamic solvation sphere may facilitate faster lithium transport.

If ion solvation dominates, systems like FSI^-/TMP, showing higher interaction energies, may improve ionic conductivity. Conversely, ion mobility, correlated to low activation energy for diffusion and high D, takes advantage of a low overall interaction energy with the Li environment, such as, maybe, in the $LiPF_6$/EC-DMC system.

In summary, it is crucial to understand which of these contributions predominates. For instance, high ion solvation can compensate for modest ion mobility in the GPE, ensuring effective diffusion. In the investigated GPE, the solubility of Li^+ is expected to be high, as the GPE incorporates a significant amount of liquid electrolyte, as reported in reference [15], and the interactions between Li^+ and the polymer function groups are not direct. Thus, we anticipate that solvation plays a significant role in the observed Li^+ transport.

However, the -CN and $-PO(OC_2H_5)_2$ functional groups in the GPE have important functions. In fact, the former is necessary to form a stable SEI at the anode interface, while the latter forms a high-quality cathode electrolyte interphase layer as well as an anti-flammability function. It is worth highlighting that the simulations performed in this work refer to the bulk of the cross-linked 3D-ADCL-PE, which is the polymeric part not in contact with electrodes.

The combined DFT and MD protocol used in this study is quite general and adaptable, especially for preparing 3D cross-linked polymers. This flexibility makes them applicable to a variety of systems where cross-linking effects are important [36]. It is worth noting that we applied this protocol to systems with linear, non-cross-linked polymer chains [37,38], showcasing their versatility. Thus, these simulations offer valuable insights into how the cross-linking influences molecular interactions and ion transport. By exploring pore formation, molecular distribution inside the polymer matrices, structural stability, and ion mobility, this approach deepens our understanding of the system under study and opens opportunities for optimizing similar polymer-based electrolyte systems for advanced Li batteries.

4. Conclusions

Using a computational approach combining MD and DFT, our study provides significant insights into the solvation behavior of Li cations in innovative 3D cross-linked gel polymer electrolytes and highlights the influence of the different components of the transport of lithium ions.

The radial distribution functions and coordination numbers obtained from long MD simulations reveal well-defined Li solvation shells predominantly involving solvent molecules and the associated PF_6^- and FSI^-. We found that Li^+ exhibits a pronounced affinity for solvent molecules and counter-anions of the electrolytes ($LiPF_6$/EC/DMC and LiFSI/TMP), while showing negligible interactions with the –CN and $-PO(OC_2H_5)_2$ polymer functional groups of the bulk polymer. This suggests that a solution-diffusion mechanism for lithium-ion transport can be assumed in these systems in agreement with the large values of the computed interaction energies.

The ΔE_{int} further indicates that the LiFSI/TMP shows more robust interactions with Li^+ than the $LiPF_6$/EC/DMC electrolyte. The last finding indicates that LiFSI/TMP more

efficiently stabilizes the Li^+ solvation shell and may improve ionic conductivity, assuming a solution-diffusion transport mechanism predominated by the solvation contribution. The $LiPF_6$/EC-DMC electrolytes, although giving lower values of ΔE_{int}, may provide enhanced ion mobility due to their looser solvation structure if the transport is controlled by diffusion contribution, but with associated stability trade-offs. Moreover, the robust interaction of Li^+ with the electrolyte constituents in LiFSI/TMP compared to $LiPF_6$/EC-DMC suggests its potential for enhanced long-term stability and safety while concurrently preserving competitive performance. It is very important to emphasize that the ΔE_{int} was calculated taking into account the effect of the polymer matrix in which the electrolytes are dispersed.

Thus, the findings remark on the significance of choosing suitable solvents and counter-anions to enhance the efficiency and safety of LiMBs using GPE. These observations can guide future research focused on optimizing the electrolyte composition in multifunctional designs and 3D cross-linking networks, specifically for solvent-salt combinations, to attain the ideal equilibrium among ionic conductivity, stability, and safety in lithium metal batteries.

Supplementary Materials: The following supporting information can be downloaded at https://www.mdpi.com/article/10.3390/batteries11010027/s1, Figure S1: (a) RDF plot referring to Li^+-F from PF6- anion, (b) and (c) referring to Li^+-O of EC and DMC solvent molecules, respectively; Figure S2: (a) Coordination Number plot referring to Li^+-F from PF6- anion, (b) and (c) referring to Li^+-O of EC and DMC solvent molecules, respectively. Figure S3: (a), (b) and (c) RDF plots referring to Li^+- F, Li^+- N, Li^+- O of the FSI-, (d) referring to Li^+-O from TMP solvent molecule, respectively. Figure S4: (a), (b) and (c) coordination number as a function of Li^+- F, Li^+- N, Li^+- O of the FSI-, (d) referring to Li^+-O from TMP solvent molecule, respectively. Figure S5. RDF plots referring to Li^+-N of ACN (a), Li^+- O from DEVP carbonyl (b), Li^+- O from DEVP ethyl (c) and Li-P of DEVP (d), respectively. It is very important to note the scale of the g(r) compared with the RDFs referring to E_1 and E_2 components. Figure S6. Coordination number as a function of Li^+-N of ACN (a), Li^+-O from DEVP carbonyl (b), Li^+- O from DEVP ethyl (c) and Li-P of DEVP (d) distances, respectively. Figure S7: RDF plots referring to Li^+-N of ACN (a), Li^+- O from DEVP carbonyl (b), Li^+- O from DEVP ethyl (c) and Li-P of DEVP (d), respectively. It is very important to note the scale of the g(r) compared with the RDFs referring to E1 and E2 components. Figure S8: Coordination number as a function of Li^+-N of ACN (a), Li^+-O from DEVP carbonyl (b), Li^+- O from DEVP ethyl (c) and Li-P of DEVP (d) distances, respectively. the 3D cross-linked polymer is soaked in the 1 M FSI-, TMP electrolyte.

Author Contributions: Conceptualization, G.D.L.; Methodology, G.D.L.; Validation, G.D.L.; Formal analysis, N.A.-H., J.L.D.S., S.A.P. and G.D.L.; Investigation, N.A.-H., P.V.S., J.L.D.S. and G.D.L.; Resources, S.A.P.; Data curation, N.A.-H., P.V.S. and J.L.D.S.; Writing—original draft, N.A.-H. and G.D.L.; Writing—review & editing, N.A.-H., P.V.S., J.L.D.S., S.A.P. and G.D.L.; Visualization, N.A.-H., P.V.S. and J.L.D.S.; Supervision, G.D.L.; Funding acquisition, S.A.P. All authors have read and agreed to the published version of the manuscript.

Funding: This research received fund from CONICET (28720210101190CO, 11220200102306CO), SECyT of the Universidad Nacional de Córdoba, and MinCyT (RESOL-2023-850-APNMCT).

Data Availability Statement: The original contributions presented in the study are included in the article and Supplementary Materials, further inquiries can be directed to the corresponding author.

Acknowledgments: This work used computational resources from CCAD-UNC. We especially acknowledge Cameron Abrams for his useful explanations about the HTPolyNet package. P.V.S. acknowledges support from a Ph.D. fellowship from CONICET. P.V.S. and S.A.P. also acknowledge other financial support from CONICET (28720210101190CO, 11220200102306CO), SECyT of the Universidad Nacional de Córdoba, and MinCyT (RESOL-2023-850-APNMCT).

Conflicts of Interest: The authors declare no conflict of interest.

References

1. Hu, Z.; Zhang, Y.; Zhang, Y.; Luo, J.; Chen, W.; Fan, W.; Huo, S.; Jing, X.; Bao, W.; Long, X.; et al. In-situ construction of high-temperature-resistant 3D composite polymer electrolyte membranes towards high-performance all-solid-state lithium metal batteries. *J. Power Sources* **2022**, *548*, 232052. [CrossRef]
2. Li, Y.; Sun, Z.; Liu, D.; Gao, Y.; Wang, Y.; Bu, H.; Li, M.; Zhang, Y.; Gao, G.; Ding, S. A composite solid polymer electrolyte incorporating MnO_2 nanosheets with reinforced mechanical properties and electrochemical stability for lithium metal batteries. *J. Mater. Chem. A* **2020**, *8*, 2021–2032. [CrossRef]
3. Xu, W.; Wang, J.; Ding, F.; Chen, X.; Nasybulin, E.; Zhang, Y.; Zhang, J.-G. Lithium metal anodes for rechargeable batteries. *Energy Environ. Sci.* **2014**, *7*, 513–537. [CrossRef]
4. Zhang, J.-G.; Xu, W.; Xiao, J.; Cao, X.; Liu, J. Lithium Metal Anodes with Nonaqueous Electrolytes. *Chem. Rev.* **2020**, *120*, 13312–13348. [CrossRef]
5. Chu, S.; Majumdar, A. Opportunities and challenges for a sustainable energy future. *Nature* **2012**, *488*, 294–303. [CrossRef]
6. Dunn, B.; Kamath, H.; Tarascon, J.M. Electrical energy storage for the grid: A battery of choices. *Science* **2011**, *334*, 928–935. [CrossRef]
7. Hwang, J.; Matsumoto, K.; Chen, C.-Y.; Hagiwara, R. Pseudo-solid-state electrolytes utilizing the ionic liquid family for rechargeable batteries. *Energy Environ. Sci.* **2021**, *14*, 5834–5863. [CrossRef]
8. Sun, M.; Zeng, Z.; Hu, W.; Sheng, K.; Wang, Z.; Han, Z.; Peng, L.; Yu, C.; Cheng, S.; Fan, M.; et al. Scalable fabrication of solid-state batteries through high-energy electronic beam. *Chem. Eng. J.* **2022**, *431*, 134323. [CrossRef]
9. Zhang, X.; Wang, A.; Liu, X.; Luo, J. Dendrites in Lithium Metal Anodes: Suppression, Regulation, and Elimination. *Acc. Chem. Res.* **2019**, *52*, 3223–3232. [CrossRef]
10. Aruchamy, K.; Ramasundaram, S.; Divya, S.; Chandran, M.; Yun, K.; Oh, T.H. Gel Polymer Electrolytes: Advancing Solid-State Batteries for High-Performance Applications. *Gels* **2023**, *9*, 585. [CrossRef]
11. Yu, F.; Zhao, L.; Zhang, H.; Sun, Z.; Li, Y.; Hu, Q.; Chen, Y. Cathode/gel polymer electrolyte integration design based on continuous composition and preparation technique for high performance lithium ion batteries. *RSC Adv.* **2021**, *11*, 3854–3862. [CrossRef] [PubMed]
12. Zhang, Z.; Huang, Y.; Li, C.; Li, X. Metal–Organic Framework-Supported Poly(ethylene oxide) Composite Gel Polymer Electrolytes for High-Performance Lithium/Sodium Metal Batteries. *ACS Appl. Mater. Interfaces* **2021**, *13*, 37262–37272. [CrossRef] [PubMed]
13. Wang, S.; Zhou, L.; Tufail, M.K.; Yang, L.; Zhai, P.; Chen, R.; Yang, W. In-Situ synthesized Non-flammable gel polymer electrolyte enable highly safe and Dendrite-Free lithium metal batteries. *Chem. Eng. J.* **2021**, *415*, 128846. [CrossRef]
14. Wang, Q.; Liu, P.; Li, S.; Wang, X.; Li, F.; Ma, J.; Chai, J.; Zhang, J.; Xu, G.; Huang, Z.; et al. A Flame Retardant Ionic Conductor Additive for Safety-Reinforced Liquid Electrolyte of Lithium Batteries. *J. Electrochem. Soc.* **2017**, *164*, A1559. [CrossRef]
15. Hu, Z.; Wang, Y.; Huo, S.; Bao, W.; Fan, W.; Zhang, Y.; Jing, X.; Ahmad, N.; Cheng, H.; Zhang, Y. Integrated design of multifunctional all-in-one polymer electrolyte membranes with 3D crosslinking networks toward high-performance lithium metal batteries. *J. Membr. Sci.* **2023**, *677*, 121643. [CrossRef]
16. Hu, Z.; Chen, J.; Guo, Y.; Zhu, J.; Qu, X.; Niu, W.; Liu, X. Fire-resistant, high-performance gel polymer electrolytes derived from poly(ionic liquid)/P(VDF-HFP) composite membranes for lithium ion batteries. *J. Membr. Sci.* **2020**, *599*, 117827. [CrossRef]
17. Wróbel, P.; Kubisiak, P.; Eilmes, A. MeTFSI (Me = Li, Na) Solvation in Ethylene Carbonate and Fluorinated Ethylene Carbonate: A Molecular Dynamics Study. *J. Phys. Chem. B* **2021**, *125*, 1248–1258. [CrossRef]
18. Tasaki, K. Solvent Decompositions and Physical Properties of Decomposition Compounds in Li-Ion Battery Electrolytes Studied by DFT Calculations and Molecular Dynamics Simulations. *J. Phys. Chem. B* **2005**, *109*, 2920–2933. [CrossRef]
19. Haskins, J.B.; Bauschlicher, C.W., Jr.; Lawson, J.W. Ab Initio Simulations and Electronic Structure of Lithium-Doped Ionic Liquids: Structure, Transport, and Electrochemical Stability. *J. Phys. Chem. B* **2015**, *119*, 14705–14719. [CrossRef]
20. Chawla, N.; Bharti, N.; Singh, S. Recent Advances in Non-Flammable Electrolytes for Safer Lithium-Ion Batteries. *Batteries* **2019**, *5*, 19. [CrossRef]
21. Shi, P.; Zheng, H.; Liang, X.; Sun, Y.; Cheng, S.; Chen, C.; Xiang, H. A highly concentrated phosphate-based electrolyte for high-safety rechargeable lithium batteries. *Chem. Commun.* **2018**, *54*, 4453–4456. [CrossRef]
22. Cats, P.; Evans, R.; Härtel, A.; van Roij, R. Primitive model electrolytes in the near and far field: Decay lengths from DFT and simulations. *J. Chem. Phys.* **2021**, *154*, 124504. [CrossRef]
23. Diddens, D.; Heuer, A. Lithium Ion Transport Mechanism in Ternary Polymer Electrolyte-Ionic Liquid Mixtures: A Molecular Dynamics Simulation Study. *ACS Macro Lett.* **2013**, *2*, 322–326. [CrossRef] [PubMed]
24. Huang, M.; Abrams, C.F. HTPolyNet: A general system generator for all-atom molecular simulations of amorphous crosslinked polymers. *SoftwareX* **2023**, *21*, 101303. [CrossRef]
25. Wang, J.; Wolf, R.M.; Caldwell, J.W.; Kollman, P.A.; Case, D.A. Development and testing of a general amber force field. *J. Comput. Chem.* **2004**, *25*, 1157–1174. [CrossRef] [PubMed]

26. Berendsen, H.J.C.; van der Spoel, D.; van Drunen, R. GROMACS: A message-passing parallel molecular dynamics implementation. *Comput. Phys. Commun.* **1995**, *91*, 43–56. [CrossRef]
27. Abraham, M.J.; Murtola, T.; Schulz, R.; Páll, S.; Smith, J.C.; Hess, B.; Lindahl, E. GROMACS: High performance molecular simulations through multi-level parallelism from laptops to supercomputers. *SoftwareX* **2015**, *1–2*, 19–25. [CrossRef]
28. Sousa da Silva, A.W.; Vranken, W.F. ACPYPE—AnteChamber PYthon Parser interfacE. *BMC Res. Notes* **2012**, *5*, 367. [CrossRef]
29. Shen, X.; Hua, H.; Li, H.; Li, R.; Hu, T.; Wu, D.; Zhang, P.; Zhao, J. Synthesis and molecular dynamic simulation of a novel single ion conducting gel polymer electrolyte for lithium-ion batteries. *Polymer* **2020**, *201*, 122568. [CrossRef]
30. Levine, B.G.; Stone, J.E.; Kohlmeyer, A. Fast analysis of molecular dynamics trajectories with graphics processing units—Radial distribution function histogramming. *J. Comput. Phys.* **2011**, *230*, 3556–3569. [CrossRef]
31. Valiev, M.; Bylaska, E.J.; Govind, N.; Kowalski, K.; Straatsma, T.P.; Van Dam, H.J.J.; Wang, D.; Nieplocha, J.; Apra, E.; Windus, T.L.; et al. NWChem: A comprehensive and scalable open-source solution for large scale molecular simulations. *Comput. Phys. Commun.* **2010**, *181*, 1477–1489. [CrossRef]
32. Hertwig, R.H.; Koch, W. On the parameterization of the local correlation functional. What is Becke-3-LYP? *Chem. Phys. Lett.* **1997**, *268*, 345–351. [CrossRef]
33. Chen, X.; Yao, N.; Zeng, B.-S.; Zhang, Q. Ion–solvent chemistry in lithium battery electrolytes: From mono-solvent to multi-solvent complexes. *Fundam. Res.* **2021**, *1*, 393–398. [CrossRef]
34. Boys, S.F.; Bernardi, F. The calculation of small molecular interactions by the differences of separate total energies. *Some Proced. Reduc. Errors. Mol. Phys.* **1970**, *19*, 553–566.
35. Simon, S.; Duran, M.; Dannenberg, J.J. How does basis set superposition error change the potential surfaces for hydrogen-bonded dimers? *J. Chem. Phys.* **1996**, *105*, 11024–11031. [CrossRef]
36. Ademmer, M.; Su, P.-H.; Dodell, L.; Asenbauer, J.; Osenberg, M.; Hilger, A.; Chang, J.-K.; Manke, I.; Neumann, M.; Schmidt, V.; et al. Unveiling the Impact of Cross-Linking Redox-Active Polymers on Their Electrochemical Behavior by 3D Imaging and Statistical Microstructure Analysis. *J. Phys. Chem. C* **2023**, *127*, 19366–19377. [CrossRef]
37. Luque Di Salvo, J.; De Luca, G.; Cipollina, A.; Micale, G. Effect of ion exchange capacity and water uptake on hydroxide transport in PSU-TMA membranes: A DFT and molecular dynamics study. *J. Membr. Sci.* **2020**, *599*, 117837. [CrossRef]
38. Luque Di Salvo, J.; De Luca, G.; Cipollina, A.; Micale, G. A full-atom multiscale modelling for sodium chloride diffusion in anion exchange membranes. *J. Membr. Sci.* **2021**, *637*, 119646. [CrossRef]